10. NONDESTRUCTIVE EVALUATION

A. Nondestructive Evaluation (NDE) Inspection of Resistance Spot Welds in Automotive Structures Using an Ultrasonic Phased Array

Principal Investigator: Deborah Hopkins, Ph.D.
Lawrence Berkeley National Laboratory (LBNL)
1 Cyclotron Road, MS 46A-1123, Berkeley, CA 94720
(510) 486-4922; fax: (510) 486-4711; e-mail: dlhopkins@lbl.gov

Technology Area Development Manager: Joseph Carpenter
(202) 586-1022; fax: (202) 586-1600; e-mail: joseph.carpenter@ee.doe.gov

Expert Technical Monitor: Philip S. Sklad
(865) 574-5069; fax: (865) 576-4963; e-mail: skladps@ornl.gov

Contractor: LBNL
Contract No.: DE-AC03-765F0095

Objective

- Develop a cost-effective, ultrasonic phased-array system that is sufficiently fast to inspect and accurately analyze spot welds in a few seconds, that is also robust enough to be used in manufacturing environments.

Approach

- Work in conjunction with the U.S. Automotive Materials Partnership's (USAMP) AMD 409 project to set technical specifications, define the technical approach and evaluate results.
- Develop a spot-weld inspection system based on state-of-the-art ultrasonic phased-array technology that can be used by operators with minimal training.
- Develop the hardware and software necessary to allow resistance spot welds (RSWs) to be ultrasonically imaged and automatically assessed in a few seconds.
- Design and fabricate a fully-integrated prototype system that is as lightweight, portable and ergonomic as possible, that is also rugged enough for use in a production facility and flexible enough to ensure access to welds on complex components.
- Conduct validation experiments to demonstrate the prototype system's ability to characterize welds with sufficient accuracy and repeatability.
- For mild and low-carbon steel, develop a fundamental understanding of the relationships among micro-structure, weld strength, the size of the weld nugget and weld button, and ultrasonic transmission across the welding interface. Determine how these relationships are affected by surface coatings, unequal-thickness stackups, teardown methods and differences in alloys.

Accomplishments

- Designed and fabricated a portable, integrated probe housing that maintains the phased-array probe in water, contains a miniature mechanical system that allows linear translation of the probe, and provides an outer membrane that confines the water column while also providing acoustic coupling to the part under inspection. Identified and tested commercially-available coupling materials that allow satisfactory signals to be obtained outside of a water tank.

- Demonstrated the ability to acquire more than 4,000 signals per weld and analyze the resulting data in a few seconds to render an estimate of weld quality. Demonstrated good correlation between ultrasonic measurements and metallographic images.
- Developed signal and image-processing algorithms that allow dimensional analysis of welds. Demonstrated the ability to accurately predict the size of weld buttons from the ultrasonic data, and the repeatability of the predictions. Developed a method to accurately quantify the uncertainty in the predictions at the size threshold that separates satisfactory from undersized welds. This value is the upper 95% confidence interval at the threshold, and ranges between 0.4 and 0.8 mm depending on the stackup (relative sheet thicknesses and material properties) and whether or not indentation variables are used in the prediction model.
- Developed a better understanding of how metallurgy, coatings, and stackup affect creation of welds, weld strength and transmission of ultrasonic energy across the welding interface.

Future Direction

- Complete a comprehensive report detailing the work and conclusions drawn from the research performed to date to determine the technical feasibility of using ultrasonic phased arrays for inspection of RSWs in steel.
- Using the hardware and software developed for inspection of spot welds in mild steel, develop inspection protocols for welds in other automotive materials such as Al and advanced high-strength steel (AHSS).

Introduction

In previous work, a prototype ultrasonic phased-array inspection system was designed and built for inspection of RSWs. The system integrates a commercial phased-array probe and controller with custom hardware and software to provide high-resolution images of the welds. The portable probe housing maintains the phased array in water, contains a miniature mechanical system that allows linear translation of the probe, and provides an outer membrane that confines the water column while also providing acoustic coupling to the part under inspection (Figure 1). Close to 4,000 signals per weld are acquired and analyzed in a few seconds to render an estimate of weld quality and size. The prototype system has been used to conduct measurements on both production parts and test coupons provided by industry partners.

The work performed during fiscal year (FY) 2007 had three main thrusts: 1) improving models used to predict the size of weld buttons from the ultrasonic data, evaluating the prediction uncertainty of these models, and assessing the repeatability and reproducibility of measurements made with the prototype spot-weld inspection system; 2) understanding the mechanics and metallurgy of weld formation in coated steel (mild and interstitial free) to better understand the relationship between the microstructure in the weld zone and the transmission of ultrasonic energy across the welding interface; and 3) understanding the stackup dependence in ultrasonic measurements.

Measurements and Signal Processing

The results presented here were obtained using an 80-element, 17-MHz, linear phased-array probe with curved elements that create a natural focal length of 37 mm. Electronic focusing is used in the direction perpendicular to the mechanical focusing to achieve a relatively small focal spot that is scanned through the weld. The miniature mechanical scanner integrated into the probe housing is used to translate the probe in the direction perpendicular to the electronic scan to create two-dimensional images of the weld.

The ultrasonic signals are analyzed in the frequency domain, where the relative magnitude of the peaks in the power spectrum is indicative of the amount of energy reflected at the interface between the welded sheets. For a satisfactory weld, most of the ultrasonic energy propagates through the weld resulting in a peak that corresponds to the travel path through both sheets. For discrepant welds, where most of the energy is reflected at the interface between the two sheets, there is a peak in the spectrum that corresponds to a travel path equal to twice the thickness of the upper sheet. For each of the 3,900 signals that comprise each weld image, the ratio of the peaks in the power spectrum is calculated. The signals are amplified by the material attenuation rate to make data obtained for different thickness sheets more comparable. The resulting amplified frequency ratio (AFR) images are displayed in the following figures. Weak signals, that cannot be analyzed, are also displayed and serve two functions. The first is to provide information on the quality of the data and the second is to provide diagnostic feedback (large areas of weak signals surrounding the weld are indicative of a burnt weld). In sizing the weld and analyzing quality, the best results are achieved by extracting several diagnostic features from the data. The contiguous area over which there is transmission across the interface (above a threshold) is calculated, and the frequency ratio is integrated over this area to obtain the integrated amplified frequency ratio (IAFR). The surface indentation caused by the welding electrode on the measurement surface is also calculated and the depth, shape, and inclination of the indentation provide useful process feedback.

Figure 1. Integrated probe being used to inspect welds on a truck door.

Results of Mechanical Testing

In one of the two studies described here, eight spot-welded test coupons were created in each of 15 weld groups by the Ford Motor Co. For seven of the groups, the coupons consisted of equal-thickness (1 mm) sheets of galvanized steel, and for the other eight groups the test specimens were composed of unequal-thickness sheets (1.0:1.45 mm). Within each group, welding parameters were held constant, and between groups they were varied to create a range of weld qualities from very weak welds to burnt welds. After ultrasonic measurements were performed, three welds from each group were subjected to lap-shear tests, two were subjected to coach-peel tests, two were sectioned and etched for metallographic analysis, and one was left undamaged to be available for future work. For the welds subjected to destructive testing, the resulting weld buttons (if any) were measured. The size of the button is sensitive to the way the load is applied, so button measures from different tests are not directly comparable. AFR ultrasonic images along with the force-displacement curves obtained for the same welds are shown in Figure 2 for four welds subjected to lap-shear testing, and in Figure 3 for four welds subjected to coach-peel testing. The strength measures derived from the curves are the peak load attained and the total area under the curve. The average button diameters and ultrasonic IAFR values for the same welds are listed in Table 1. The lap-shear and coach-peel results differ in both the peak loads and post-peak behavior, but in both cases the force-displacement curves show a progression in mechanical behavior.

The weakest welds pull apart under almost no load (e.g., weld E6). For somewhat stronger welds, the force-displacement curves indicate little if any strength after the peak load (e.g., weld M1). Even though neither weld M1 nor L1 pulled a button in lap shear, suggesting interfacial failure, the force-displacement curves show a transition toward more ductile behavior for weld L1 (Figure 2). The ultrasonic IAFR values are similar for the two welds (Table 1), but what is visible in the AFR images is a transition from dispersed areas of transmission across the interface to a more uniform contiguous area of high transmission. Weld O1 is a borderline-good weld, and while there is not much increase in peak load compared to the weaker welds, the weld demonstrates increased ductility and a substantially higher IAFR value. The fourth weld in the series (H1) is a satisfactory weld that sustained a higher peak load, with much more area under the force-displacement curve and a high IAFR value compared to the smaller welds.

For the welds tested in coach peel (Figure 3), the button pulls out of the parent material of one of the sheets. Weld E6 was very weak, and the AFR image shows that fusion initiated along a ring. Weld D6 is an undersized weld, with a force-displacement curve that is characteristic of undersized and satisfactory welds. Weld G8 is a large weld and A7 is a burnt weld; in both cases, there is a transition from ductile to more brittle behavior as evidenced by the relatively sharp peaks in the force-displacement curves. The black pixels evident in the AFR images outside of the welded region for these two welds indicate weak signals that suggest interfacial bonding characteristic of very large and burnt welds. Burnt welds are easily identified from the ultrasonic data, not only because of the weak signals, but also because of large transmissive areas, high IAFR values and excessively- deep surface indentations.

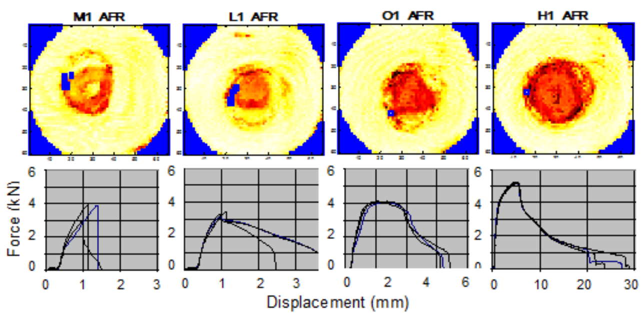

Figure 2. AFR ultrasonic images (top row) and the corresponding force-versus-displacement curves for all welds in the same group for four welds subjected to lap-shear strength testing (note that the x-axis scales differ). The button dimensions and IAFR values obtained for the same welds are reported in Table 1.

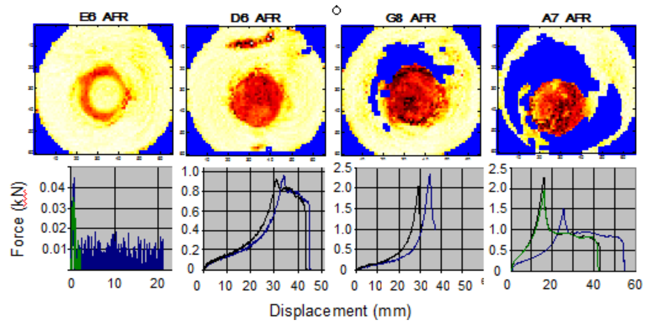

Figure 3. AFR ultrasonic images (top row) and the corresponding force-versus-displacement curves for all welds in the same group for four welds subjected to coach-peel strength testing (note that the axes scales differ). The large dark areas in the AFR images for G8 and A7 are indicative of burnt welds. The button dimensions and IAFR values obtained for the same welds are reported in Table 1.

Table 1. Button sizes and ultrasonic IAFR values for welds tested in lap shear and coach peel.

Lap-shear strength tests (sheet-metal stackup 1.0:1.45mm)				
	Weld M1	Weld L1	Weld O1	Weld H1
Ave. button diameter	No button	No button	3.3 mm	5.5 mm
Ultrasonic IAFR	353	348	718	1119
Coach-peel strength tests (sheet-metal stackup 1.0:1.0mm)				
	Weld E6	Weld D6	Weld G8	Weld A7
Ave. button diameter	No button	3.6 mm	6.2 mm	8.0 mm
Ultrasonic IAFR	243	925	1346	4604

Comparison of Ultrasonic and Metallographic Images

For the Ford study, two welds from each of the 15 groups were sectioned in the plane of the sheet metal to create planar sections at the welding interface that were subsequently polished and etched with picral to reveal the microstructure. These metallographic maps are particularly useful because they are in the same plane as the images created from the ultrasonic measurements (see Figure 4). For those welds that were sectioned, the size of the weld nugget was measured in the images and compared to the ultrasonic data. The dimensioned box in the metallographic image in Figure 4 is the heat-affected zone (HAZ). The weld nugget is the smaller circular region, which has a finer grain structure than the HAZ. The sheet metal used for the Ford samples had a very low carbon content, and the result is ferrite grain growth in the outermost region of the HAZ. As shown in the figure, the area over which there is ultrasonic transmission across the welding interface corresponds very closely to the HAZ.

For the second study discussed here, test coupons were made by General Motors (GM). In this case, the samples were made with three different sheet-metal stackups: thin-thin (sheet thickness equal to 0.8 mm); thick-thick (sheet thickness equal to 1.8 mm); and thin-thick. The thin sheets were interstitial-free (IF) low-carbon steel, and the thick sheets were mild steel. For each of the three stackups, there were five target weld classes: stick, small, undersized, minimum acceptable, and large. Following ultrasonic inspection of the welds, the samples were peeled apart to determine the weld quality as indicated by the size of the weld button.

Each of the samples was then sectioned vertically with respect to the welding interface, polished and etched with picral to reveal the weld nugget and the microstructure in and around the welds.

Micrographs for the thin-thin stackup are shown in Figure 5 for four welds targeted to be undersized.

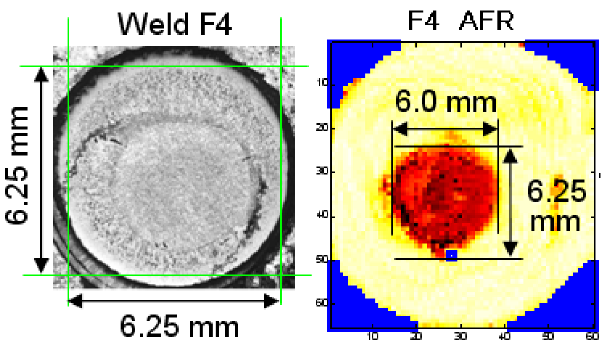

Figure 4. Metallographic planar section of a satisfactory weld (left-hand image) and the ultrasonic AFR image for the same weld (right-hand image).

The cross-sections were taken through the weld buttons, which in this case all pulled out of the upper sheet. The upper dimensions in the images are of the buttons. The smaller dimension in each of the images corresponds to the weld nugget (martensite), which is easy to see because of the thin white outline. The line is the result of carbon segregation that occurs during the first phase of solidification, during which carbon migrates into the melt zone. The picral etch is sensitive to carbon content, and thus marks the carbon-depleted line. The whitish area surrounding the nugget is a two-phase (ferrite and austenite) region of the HAZ. In the first image (weld 16), it is possible to see long ferrite grains in the outer area of the HAZ that show up relatively dark compared to the two-phase zone and the parent material. These long grains are characteristic of IF steel and do not usually occur in mild steel.

Three of the four welds were sectioned along the short axis of the samples, as indicated by the rectangles in the upper-left corner of the micrographs. The images for these welds (welds 16, 18 and 19) show relatively small nuggets and buttons. The weld sectioned in the perpendicular direction (weld 17) has a larger button and nugget, and a more typical image for an undersized weld. Recall that all four welds were made under identical conditions with the same welding parameters, suggesting something in the setup that created misshapen welds. The corresponding ultrasonic AFR images are also shown in the figure. The approximate positions of the cross-sections are indicated by the long black lines. Consistent with the micrographs, the AFR images show a large band of reflectivity at the top of the images indicating a lack of fusion. The size of the buttons compared to the nuggets for welds 16, 18 and 19 show that there is a relatively-strong, solid-state bond at the interface outside of the nugget. For welds 16, 18 and 19, where there is a large difference in size between the button and nugget, the micrographs show that the zone of high ultrasonic transmission corresponds very closely to the dimension that includes the nugget and the strong interfacial bond surrounding the nugget.

An important objective of this year's work was to better understand the relationship between the ultrasonic signals and the interfacial solid-state bonds that vary in strength from extremely weak to very strong. Micrographs and the corresponding AFR images are shown in Figure 6 for large welds in thin-thin (left-hand side) and thick-thick stackups (right-hand side). The images indicate that the signals are sensitive, at least in some cases, to conditions that affect the strength of interfacial bonds. The micrograph for weld 69 in the thin-thin stackup shows an annular weld. Because the strength of the weld is relatively insensitive to the quality of the weld in the center, these "donut" welds are considered satisfactory. In this case, the ultrasonic signals suggest that the interfacial bond in the center is very strong, transmitting the acoustic energy as well as the surrounding nugget material. In contrast, the micrograph for weld 62 in the thick-thick stackup indicates that the nugget had a plane of weakness on the left-hand side, probably resulting from porosity and voids in the nugget on the left-hand side). The corresponding ultrasonic AFR image indicates that the signals were sensitive to the weakness in the nugget. The zone of high ultrasonic transmission corresponds to the button diameter, which does not include the section of the nugget that failed.

Stackup Dependency

The modeling results in the next section show that the relationship between the weld button and ultrasonic variables varies depending on the sheet-metal stackup. One objective of this year's work was to better understand this dependency. The most difficult sample set analyzed to date is the GM thin-thick stackup (0.8:1.8mm). Figure 7 shows metallographic images, photographs of the buttons and the corresponding ultrasonic AFR images for five welds from this group. In all cases, the nuggets formed in the thick sheet at the

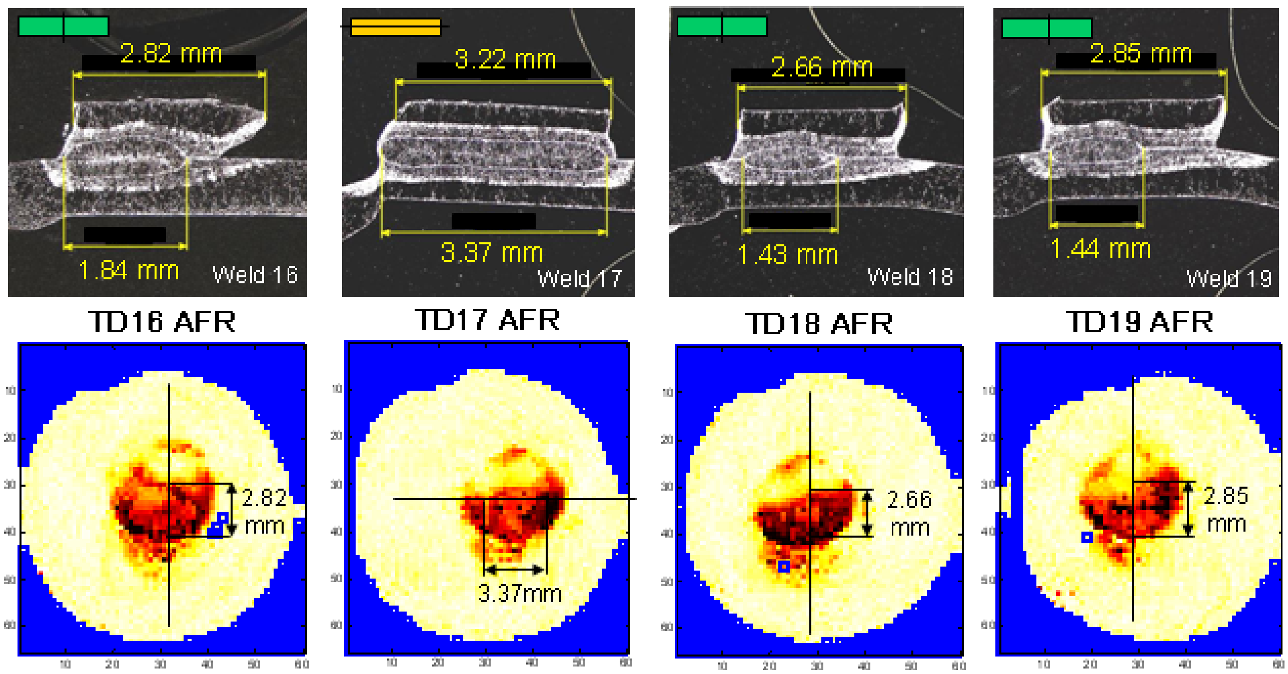

Figure 5. Micrographs and ultrasonic AFR images for four undersized welds. The rectangles in the upper-left corner of the micrographs (top view) and the black lines in the AFR images indicate the approximate location of the cross section.

geometric center of the stackup. Note that there is very little if any penetration of the weld nugget across the welding interface except for the largest welds. Nonetheless, the undersized and minimum-acceptable welds pulled relatively large buttons, and the AFR images for all but the weakest of these welds show transmission of the ultrasonic energy over a large area indicating a strong solid-state bond at the interface. As explained by Dr. Jerry Gould of the Edison Welding Institute, for coated steels, the melting and expulsion of the zinc coating leaves behind clean surfaces relatively free of oxides, thereby facilitating creation of the solid-state bonds. The fact that the nugget initiates at the geometric center of the stackup strongly indicates that these solid-state bonds conduct heat, eliminating the resistance at the welding interface. The lack of penetration of the nuggets across the faying surface is attributed to two factors. Given that the nugget initiates at the center of the stackup, the large difference in thickness (0.8 versus 1.8mm) between the two sheets requires a large nugget to even reach the welding interface. The second factor that inhibits penetration of the nugget across the interface is the difference in material properties between the sheets. The thin, IF-steel sheet is twice as conductive as the thick, mild-steel sheet. In essence, the stackup can be described as a conductor sitting on top of an insulator. This difference in conductivity is thought to foster creation of very strong solid-state bonds. The ultrasonic AFR images for these welds show that there was substantial transmission of acoustic energy across the welding interface for all welds regardless of target quality, supporting the hypothesis that the stackup geometry and difference in conductivity resulted in strong solid-state bonds that formed in conjunction with the weld nugget. Also note the voids visible in the nuggets for the three largest welds. These voids are also visible in the AFR images. At higher magnification, it is also possible to see porosity and cracking in the nuggets. In general, the presence of voids in the nugget increases with increasing sheet thickness.

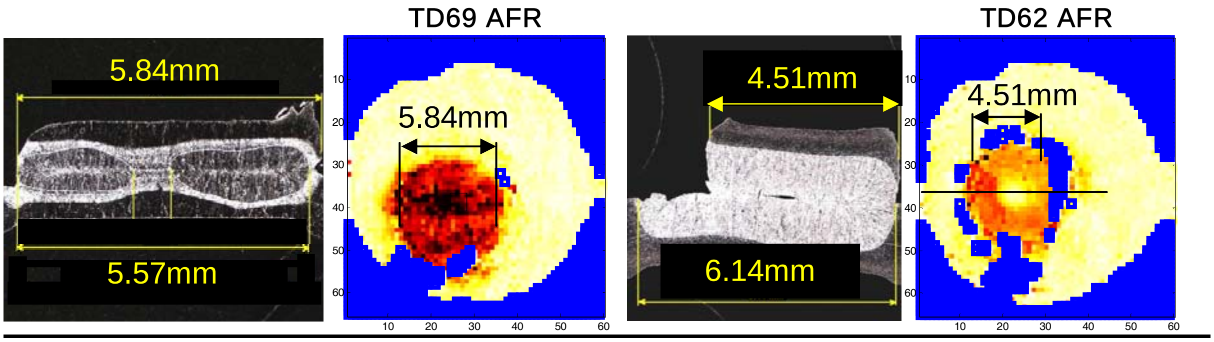

Figure 6. Micrographs and ultrasonic AFR mages for two large welds for thin-thin (left-hand side) and thick-thick stackups (right-hand side). The black lines in the AFR images indicate the approximate location of the cross section.

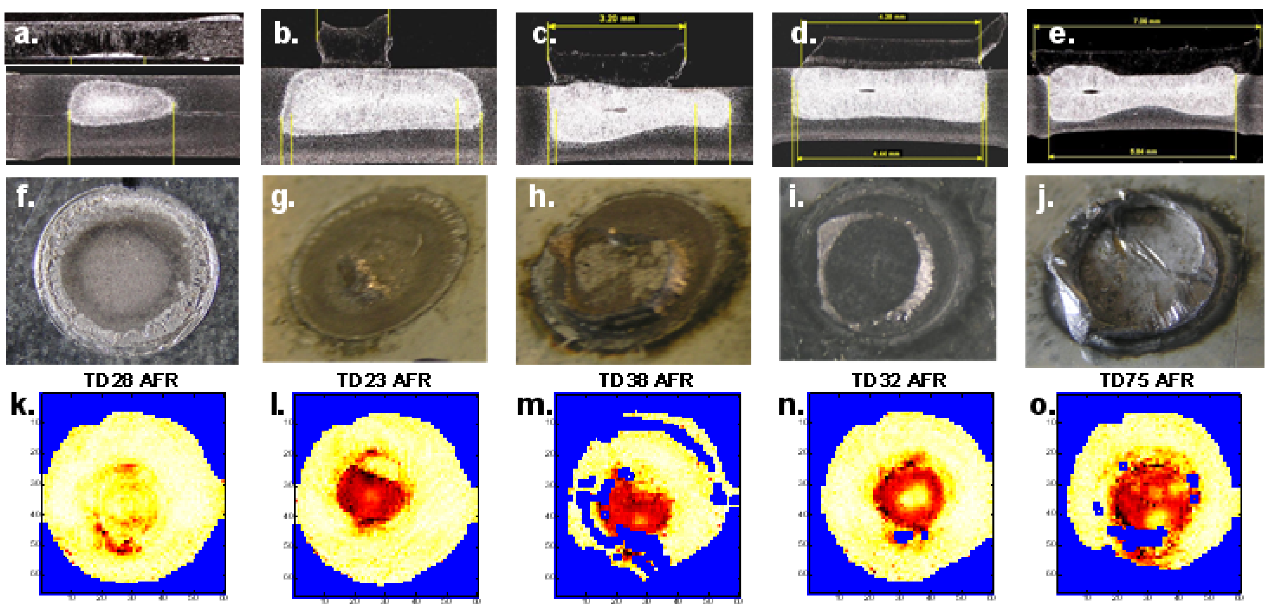

Figure 7. Metallographic cross-sections, pictures of weld buttons and ultrasonic AFR images for five welds in the thick-thick stackup with targeted qualities: stick, small, undersized, minimum acceptable, and large.

Prediction of Weld Size

To predict weld size, several step-wise regression models were estimated. The dependent variable in the regressions is based on the measurements of the weld button or, in the case of the welds sectioned by Ford, the size of the nugget identified in the metallographic image. For the step-wise technique used, variables are introduced sequentially based on a selection criterion that estimates their contribution to prediction performance. The candidate variables are all derived from the ultrasonic signals: the area over which there is transmission across the interface (TA); the IAFR, the average indentation depth (ID) and indentation area (IA).

Ideally, the variables included in the models and their order of inclusion would be identical regardless of material thickness and stackup. The Ford models are more similar to each other than the GM models both in the ultrasonic variables included and in the R^2 values obtained. The Ford data also show less stackup dependence and little is gained from using the indentation information. In contrast, there is a strong stackup dependence in the GM data and, in some cases, adding the indentation variables substantially improves the model fits. As described above, the stackup dependence in the GM data is attributed to the greater difference in relative thickness in the thin-thick stackup for the GM samples and the difference in material properties between the IF and mild steel used in the GM coupons. The regressions were run for the data broken out by stackup, and also for the data pooled across stackups. The best results are obtained using linear regression with quadratic terms, although for the Ford data, the results were nearly identical using only linear terms.

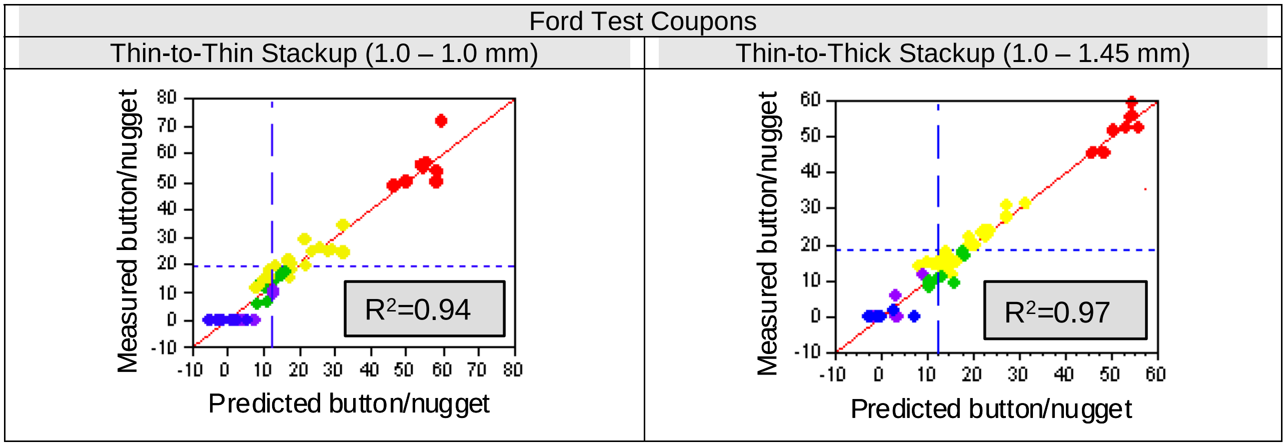

Figure 8. Measured versus predicted button areas for the full model using IAFR, TA, ID, and IA. As shown in the figures, the R^2 values for the full model are 0.94 and 0.97 for the thin-thin and thin-thick stackups, respectively. The corresponding values for the restricted model that excludes the indentation variables are 0.94 and 0.95, respectively.

One of the outputs of the regressions is the R^2 value, which is a measure of the goodness-of-fit of the model ranging between 0 and 1 (a perfect fit). In all cases, the R^2 values indicate excellent model fits. For the Ford data broken out by stackup, the R^2 values (adjusted for the number of variables in the model) are 0.94 and 0.97 for the models using indentation information (Figure 8), and 0.94 to 0.95 when the indentation variables are excluded. For the GM data by stackup, the adjusted R^2 values range from 0.96 to 0.98 for the models using indentation information (Figure 9), and from 0.90 to 0.96 when the indentation variables are excluded. For the Ford data pooled across stackups, the R^2 values are 0.96 and 0.93 for the models with and without indentation variables, respectively. The corresponding numbers for the GM data are 0.92 and 0.81.

To help evaluate the performance of the models, the prediction error at the size threshold that separates undersized from satisfactory welds was calculated based on the width of the confidence interval for the prediction equation at the threshold. This calculation answers the question as to how much larger than the threshold the welds have to be made or measured to ensure with 95% confidence that all welds predicted to be satisfactory are in reality larger than the threshold. This value ranges between 0.8 and 1.2 mm for the Ford data, and 0.4 and 0.8 mm for the GM data, for all stackups and both models (using indentation data and excluding it). The larger margin for the Ford data is not surprising given that the measured data was obtained using three different teardown methods.

Repeatability and Reproducibility

The GM welds were measured by three operators, from both the front and back sides of the samples. An additional set of measurements was made by Operator 1 from the top side in a water tank. The ultrasonic AFR images obtained by Operator 1 for four welds are displayed in Figure 10. In general, there is excellent qualitative agreement among the AFR images for repeat measurements. For example, the images for weld 28 (top row, first four images), is one of only two welds in this dataset that shows the ultrasonic signature that has in the past been associated with cold welds. The ability to reliably identify these welds is critical, since they are very weak. A quantitative evaluation of repeatability is only preliminary because of the small sample, but shows good repeatability of both predictions of weld quality and of the ultrasonic variables input into the prediction equations. AFR images obtained by the three operators for weld 40 are shown in Figure 11, along with the images obtained by Operator 1 in a water tank. Again there is in general good qualitative agreement among the images.

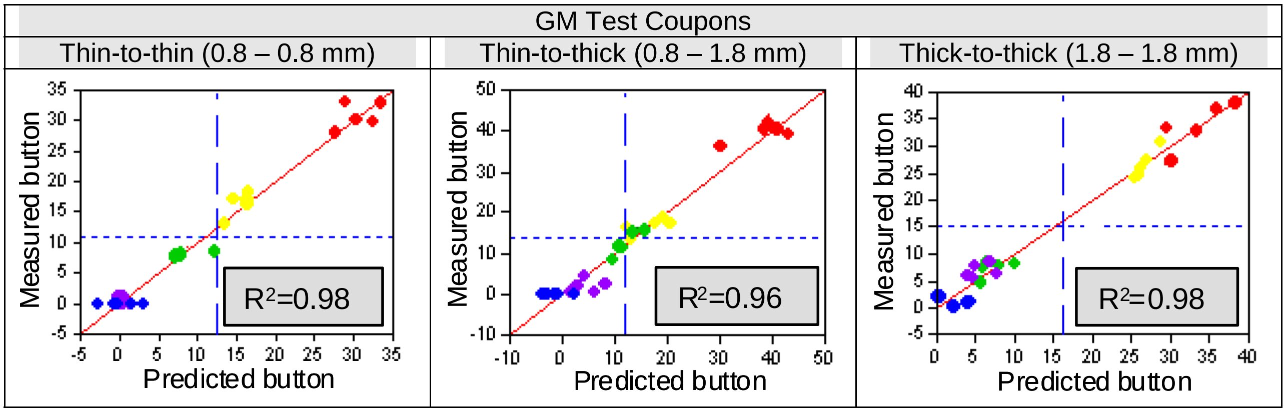

Figure 9. Measured versus predicted button areas for the full model using IAFR, TA, ID, and IA. The R^2 values for the full model are 0.98, 0.96 and 0.98 for the thin-thin, thin-thick and thick-thick stackups, respectively. The corresponding values for the restricted model that excludes the indentation variables are 0.96, 0.95, and 0.90, respectively.

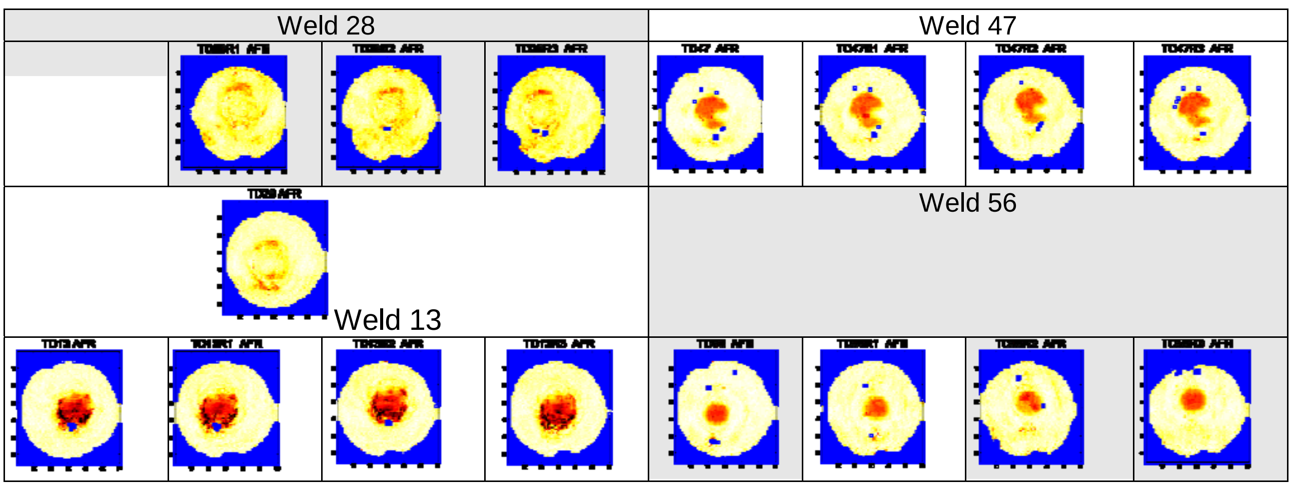

Figure 10. AFR images for the repeat measurements made by Operator 1 on four welds.

Exceptions occur in those cases where there are many weak signals, which can indicate a coupling problem. Also encouraging is the good agreement between the measurements made in the water tank and those made with the portable probe unit. The variability of the predictions made by Operators 2 and 3 is larger than that for Operator 1. Variability is greatest for Operator 2, who did not attempt to orient the probe to maximize the signal amplitude.

Conclusions

The relationships among weld strength, the size of the weld nugget and button, and ultrasonic data are complex, and depend on the sheet-metal stackup and material properties. Metallographic images are invaluable in helping to understand these relationships and their dependence on microstructure.

Force-displacement curves obtained during strength testing show a transition from brittle behavior for the weakest welds, to ductile behavior for satisfactory welds, back to more brittle-like behavior for burnt welds. Ultrasonics can identify the weakest welds and burnt welds, and can also provide information on weld shape, voids, cracks, and surface indentation, all of which are useful feedback to the welding process.

For coated steels, the melting and expulsion of zinc acts to clean the welding interface, fostering the creation of solid-state bonds. These bonds form either as a precursor to nugget formation in the case of equal-thickness sheets, or in conjunction with nugget formation in unequal-thickness sheets. The strength of solid-state bonds varies from weak to very strong. Unequal-thickness stackups and welds in dissimilar materials contribute to creation of strong solid-state bonds. All but the weakest of these welds and bonds transmit acoustic energy across the interface between the welded sheets. It has also been shown that solid-state bonds can pull a button. The existence of these bonds is, therefore, a complication for both destructive and nondestructive testing. At least in some cases, ultrasonic signals are sensitive to the strength of the solid-state bond.

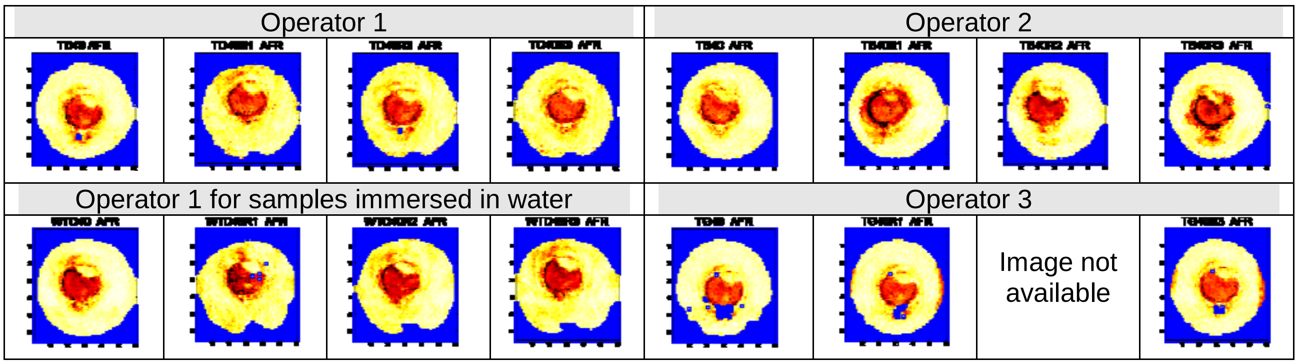

Figure 11. AFR images for repeat measurements made by three operators on weld 40, and a fourth set of measurements made on the same weld by Operator 1 for test coupons immersed in a water tank.

The best results for sizing welds is obtained using the IAFR along with other diagnostic variables extracted from the ultrasonic signals. The repeatability and reproducibility results for the GM data are encouraging, but preliminary because of the relatively small number of repeat measurements. Future work would benefit from using experimental designs that would allow gage repeatability and reproducibility (R&R) to be assessed according to industry protocols.

Measurements performed on hundreds of welds strongly indicates that sizing and assessing weld quality are more complex than simply identifying and measuring the zone of ultrasonic transmission across the welding interface. Understanding how the acoustic signals are affected by the microstructure in the weld zone is, therefore, key for determining both the capabilities and limitations of ultrasonic weld characterization.

Comparison of the results obtained using the prototype system with a coupling membrane to data obtained from measurements made by immersing the coupons in a water tank indicates that the membrane is not introducing significant error into the measurements. This result supports the feasibility of applying phased-array technology in production. Experiments to date also show that acceptable measurements can be made using inexpensive, off-the-shelf membrane materials, and that these materials are very durable, results that further improve the feasibility of using the technology in plants.

Presentations

1. D. Hopkins and W.B. Davis, “Ultrasonic Phased-Array Signal Processing for Resistance-Spot-Weld Inspection,” Automotive Industry Advancements with NDT, American Society for Nondestructive Testing, May 2007, Dearborn, MI.
2. D. Hopkins, “Development of an Ultrasonic Phased-Array System for Nondestructive Evaluation of Resistance Spot Welds,” United States Automotive Materials Partnership (USAMP) — Automotive Materials Division (AMD) Joining Offsite, November 2007, Southfield, MI.
3. W.B. Davis, "Predicting Spot Weld Button Area with an Ultrasonic Phased Array," 34th Annual Review of Progress in Quantitative Nondestructive Evaluation, August 2007, Golden, CO.

4. D. Hopkins, “Use of Metallographic Analysis and Strength Testing to Improve Ultrasonic Phased-Array Evaluation of Resistance Spot Welds,” 34th Annual Review of Progress in Quantitative Nondestructive Evaluation, August 2007, Golden, CO.
5. D. Hopkins, “Reliability in High-Volume Manufacturing — An Automotive Perspective,” American Society for Nondestructive Testing Fall Conference, November 2007, Las Vegas, NV.

Publications

1. W.B. Davis, "Predicting Spot Weld Button Area with an Ultrasonic Phased Array," To appear in *Proc. 34th Annual Review of Progress in Quantitative Nondestructive Evaluation*, 2008.
2. D. Hopkins, “Use of Metallographic Analysis and Strength Testing to Improve Ultrasonic Phased-Array Evaluation of Resistance Spot Welds,” To appear in *Proc. 34th Annual Review of Progress in Quantitative Nondestructive Evaluation*, 2008.
3. D. Hopkins and USAMP NDE Steering Committee, “Reliability in High-Volume Manufacturing — An Automotive Perspective,” feature article in *Materials Evaluation*, American Society for Nondestructive Testing, December 2007.

B. Nondestructive Inspection of Adhesive Metal/Metal Bonds (NDE 601[i])

Principal Investigator: David G. Moore
Sandia National Laboratories (SNL)
P.O. Box 5800, MS 0863
Albuquerque, NM 87185
(505) 844-7095; fax: (505) 844-9068; e-mail: dgmoore@sandia.gov

Principal Investigator: Joseph DiMambro
SNL
P.O. Box 5800, MS 0340
Albuquerque, NM 87185
(505) 284-8914; fax: (505) 844-7011; e-mail: jdimamb@sandia.gov

Principal Investigator: Cameron J. Dasch
General Motors Research & Development
30500 Mound Road, Warren MI 48090
(586) 986-0588, fax: (586) 986-3091; e-mail: cameron.j.dasch@gm.com

Technology Area Development Manager: Joseph A. Carpenter
(202) 586-1022; fax: (202) 586-1600; e-mail: joseph.carpenter@ee.doe.gov

Field Project Officer: Aaron D. Yocum
(304) 285-4852; fax: (304) 285-4403; e-mail: aaron.yocum@netl.doe.gov

Expert Technical Monitor: Philip S. Sklad
(865) 574-5069; fax: (865) 576-4963; e-mail: skladps@ornl.gov

---

Contractor: U.S. Automotive Materials Partnership (USAMP)
Contract No.: DE-FC26-02OR22910 through the DOE National Energy Technology Laboratory

---

Objective

- The goal of this project is to identify and develop a nondestructive inspection (NDI) method(s) for adhesive-bond evaluation to be used in an automotive manufacturing environment that would foster increased confidence and use in adhesive joining. The primary objective is to identify and validate an NDI method(s) which can: 1) measure the adhesive area, 2) measure adhesive thickness, and 3) detect weak metal-to-adhesive bonds (intimate contact but which have reduced strength). Wider use of adhesive joining could result in reduced vehicle weight, increased body stiffness, and improved crashworthiness. Adhesives are also seen as a critical enabler for the joining of dissimilar materials in order to avoid corrosion from dissimilar metals.

Approach

- There are five major attributes which contribute to the strength of an adhesive bond on a metal flange: the width of the adhesive area, the adhesive thickness, the location of the bead relative to the edges of the flange, the state of cure, and the quality of the adhesion. The general approach is to develop a suite of inspection techniques that can be used on the manufacturing floor which allow all the required adhesive characteristics to be measured nondestructively. The chosen methods must be a single-side inspection that can follow a flange, navigate large changes in geometry and have spatial resolution near 1 mm. To accomplish this, there is a two-step validation process: first, successfully inspect the flat, adhesively-bonded specimens representative of automobile flanges and second, deploy the inspection method on production car bodies. The flat specimens vary in adhesive, adherent type and thickness, stackup (2-3 layers), cure state, and surface contaminants. These conditions bound the processing parameters for the adhesive assembly process. A through-transmission ultrasound inspection is performed to characterize the flat specimens and is considered a "gold standard" reference inspection method. Selected samples are also peel tested to measure bond strengths. Multiple automotive bodies-in-white (BIWs) containing a number of adhesive joints were produced by the original equipment manufacturers (OEMs) to determine whether complex geometries provide any inspection impediments and to develop body-inspection strategies. Three promising, single-sided inspection technologies for bond area, location, and thickness were studied this year. They were phased-array ultrasonics, laser ultrasonics, and pulsed thermography.

Accomplishments

- Rapid progress in this first year has produced a novel, ultrasonic phased-array imaging system that has been validated and already applied to production vehicles to answer real engineering questions. This pulse/echo system uses a custom, high-frequency, linear array in a novel probe carrier designed by the project team to scan along an adhesive bead. The system includes a position encoder and portable, closed-loop, water-circulation system. These features allow images of adhesive bonds, registered to markers on the body, to be made on the production floor. The validation included a large test suite of weld-bonded steel and aluminum (Al) coupons and a production body subsystem with embedded defects. This system surpassed the design requirements for off-line inspections and can scan at over 5 meters per minute with 1-mm resolution.
- The project team is currently working on a second-generation ultrasonic array system design that will be more adaptable to the complex geometries found on production vehicles. It will be able to inspect regions with stronger radii of curvature, smaller flange widths, and smaller confinements. This will allow a very high fraction of the bonded area on BIW's to be inspected.
- A new wedge-peel destructive test was developed to provide a high-resolution measurement of the bond strength along an adhesive bead. This uses a standard impact wedge in a fixture designed by the team. This method allows larger engineering joints up to 0.6-m long to be measured quantitatively. This method was combined with ultrasonic thickness maps to determine adhesive strength laws.
- The NDI assessment of the pulsed thermography was completed based on the inspection performance on the test coupons. Both steel and Al adhesively-bonded coupons were verified by comparing inspection results to the destructive findings.
- A reproducible procedure for constructing an intimate-but-weak ("kissing") bond samples using a grease contaminate was established. Samples with reduced shear strength were made and evaluated with an ultrasonic inspection. The resulting images could be correlated to the subsequent strength measurements.

Future Direction

- In the coming year, the second-generation ultrasonic array system will be built and evaluated, especially on the BIW structures. A major emphasis of this development will include advanced signal analysis to determine reliably the bead thickness and quality of all adhesive/adherent interfaces. These developments are geared to improve inspectibility, reduce overall system cost, increase reliability and to reach a production-ready system. The second year will also begin the process of identifying methods to detect weak bonds. These are likely to include vibrothermography, angle-beam ultrasonic spectroscopy, nonlinear ultrasonics, and laser shock peening. A mid-year report will be written addressing the advantages and disadvantages of each technique. The third year is focused on productionizing a weak-bond detection method.

Introduction

Adhesive bonding is increasing every year as automotive manufacturers strive to make bodies stiffer and stronger. Recent applications see as much as 100 meters of adhesive per vehicle being used. Adhesive joining is already widely used in automotive production today for improving body stiffness and durability, but is increasingly being used for impact performance. Current manufacturing processes for adhesive joints rely primarily on quality control of the adhesive preparation and application. Controls include machine-vision technologies to verify the applied adhesive bead before the mating piece is joined. However, there is no method currently available to test the overall quality of the final assembled joints other than destructive testing. Adhesive joining is seen as a major weight-saving technology. When adhesives are used in combination with spot welds or rivets, the resulting joints are much stiffer and stronger. Almost a doubling of shear strength has been produced in weld-bonded joints when compared with spot welds alone. Moreover, by enabling dissimilar materials to be used in close proximity to each other, assemblies can be constructed with optimized, lightweight materials such as magnesium (Mg) and Al.

A major strategy of this project is to leverage the decades of development in the aerospace sector devoted to the NDI of adhesive joints. NDI is now commonly used in aerospace manufacturing of adhesive joints, especially for composite panel joining. Entire load-bearing structures are inspected. Portable NDI methods are also used in routine, in-service aircraft inspections.

Within the automotive prototype development sector, increased inspection capability is needed. The major area of need is within the body shop before the adhesive is cured. This is the most likely place in the manufacturing steps where discrepant joints would be repaired. Additionally, inspections are also needed at the end-of-line to ensure the quality of the entire assembled, cured, and painted product. NDI inspections are also seen as a major cost savings for accelerating engineering and environmental testing, ramp-up to production, and monitoring the long-term performance of the joints.

Coupon Preparation and Characterization

Several sets of flat, adhesively-bonded specimens, representative of automobile flanges, have been generated by the automotive OEMs and adhesive suppliers to test the feasibility of NDI techniques to assess bond area and bond-line thickness. The specimens include mild steel bonded to Al and mild steel with several production adhesives. A range of adhesive production variables, thickness under compression, and both cured and uncured conditions are embedded in the samples. These variables were designed into the specimens to include as many production processes as possible. These coupon sets allowed for parallel nondestructive and destructive testing to occur within the project.

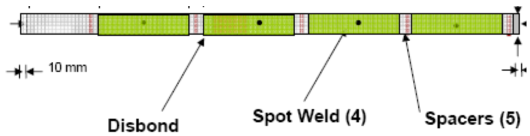

Figure 1. Joint layout prior to assembly.

An example of the coupons prior to assembly is shown in Figure 1 showing the wire spacers used to control the adhesive thickness, intentional skips, and a section of Teflon tape to simulate a kissing bond. Most of the specimens have also been spot welded using typical production welders and standard welding parameters.

All the manufactured test specimens were nondestructively inspected using high-frequency, immersion, ultrasonic through-transmission inspection method (UT-TT). The transmitted signal strength allows the areas where all interfaces in the stack are in contact with each other to be imaged (Figure 2a). Using the experimentally-measured speed of sound for each adhesive in its state-of-cure, a map of the adhesive thickness is simultaneously measured (Figure 2b). Using image analysis, the bead width and average bead thickness at each flange location can be determined. These data provide the reference for the evaluation of the other inspections.

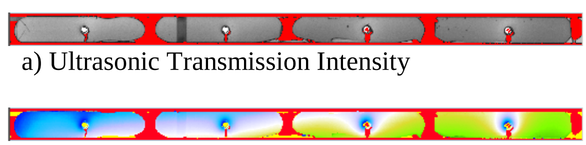

a) Ultrasonic Transmission Intensity

b) Ultrasonic Thickness Measurement

Figure 2. Ultrasonic characterization of a 600-mm long weld-bonded coupon.

A new, wedge-peel destructive test was also developed. This method uses an instrumented load frame to pull a standard wedge (ISO11343) through the adhesive bond. This produces a load-vs.-displacement curve. This method was selected after evaluating three alternative peel methods including the standard floating-roller peel, a multi-roller peel test, and a thin-slicer peel test. As seen in Figure 3, the load-versus-displacement curves have been combined with the ultrasonic bead-width and average bead-thickness measurements to determine strength laws.

The combination of nondestructive imaging with destructive tests has driven our emphasis on bead-width measurement and minimum bead-thickness detection.

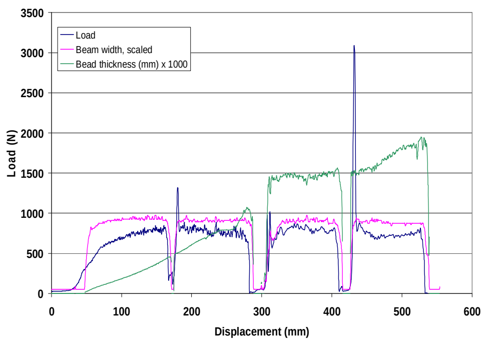

Figure 3. Wedge-peel strength measurements compared with ultrasonic bead-width and thickness measurements.

Ultrasonic Pulse/Echo Imaging

Ultrasonic pulse/echo imaging has been a standard inspection tool for adhesive inspections for many decades. A short ultrasonic pulse is launched through the outer adherent and the train of echoes from the various adhesive-adherent interfaces is detected. Typically, the ultrasonic beam is raster-scanned over the bond area and variations of the interface reflectivity are used to determine the joint condition. The primary barriers to introducing this to the plant floor have been the complex joint geometries and the difficulty of analyzing the ultrasonic echoes. This year, three different pulse/echo inspections have been used in this project. Traditional raster scans in an immersion tank have been used to obtain high-quality data on flat samples for signal-analysis development. For a manufacturing tool, both a phased-array scanner and a laser-ultrasonic scanner have been under development.

Phased-array (PA) probes are comprised of many small piezoelectric elements embedded into a polymer base material. Each ultrasonic element is individually wired, allowing individual delays (phasing) to be applied to each element. This delay allows the ultrasonic beam to be steered and focused and for the reflected signals from each element to be coherently added. Linear arrays with 16 to 128 elements are commonly available, but square and circular arrays have been made for special applications. This technology also has the ability to introduce both longitudinal and shear waves simultaneously into a specimen.

A phased-array holder/scanner was designed by SNL and the United Sates Council for Automotive Research (USCAR) Design Team [1]. The probe holder has been designed specifically to rapidly inspect long and narrow flanges that may be flat or have tight radii of curvatures. The unit uses a high-frequency linear array that spans the flange width and produces a focused ultrasonic beam that is rapidly scanned electronically at up to 10,000 points per second. This probe is manually scanned along the flange or inspection area. The probe holder incorporates a position encoder so that a two-dimensional (2D) image is obtained. Figures 4 and 5 show the version 1 prototype probe and the water delivery system.

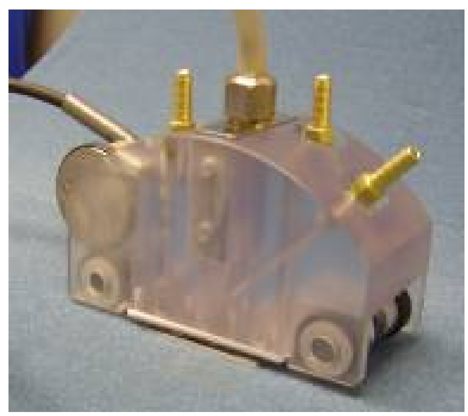

Figure 4. High-frequency phased array embedded in a custom probe holder (Version 1).

Figure 5. Phased-array probe holder on a test coupon.

The holder uses a closed-loop water-circulation system to maintain a water column between the array and the flange surface. Two angled inlet ports supply water to the array while the two vertical ports vacuum excess water from the part. The closed-loop circulation system was designed and built to include a filtered water supply, returnpump and coupling gages in a self-contained shipping case.

The system has been validated in a C-scan mode using simple time-gating in order to inspect the first adherent/adhesive interface. This provides a rapid, high-resolution scan of the adhesive-bead position and area. The system can scan at up to 10 meters per minute with 1-mm resolution. This is more than enough to inspect 100 meters of adhesive in an off-line, two-hour inspection window. The system performance was validated on flat test specimens and large BIW samples. Images demonstrating the high-resolution performance are shown in Figures 6 and 7. The PA resolution is comparable to an ultrasonic inspection using an immersion tank, i.e., about 1 mm.

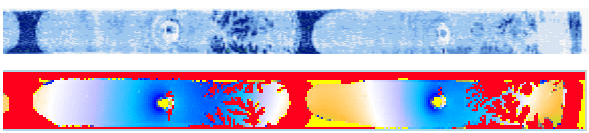

Figure 6. Phased-array image (top) of a 300-mm x 25-mm section of a coupon compared to the UT-TT reference thickness map (bottom). Note: spring-back feathering.

Deployment of the PA Probe on BIW Test Samples

After tests of embedded discrepancies such as shown in Figure 7, the scanner was deployed on BIW vehicles (Figure 8). This shows multiple adhesive maps taken of the adhesives beads between the roof-bows and the roof. This is shown for illustrative purposes since features can be readily identified. The PA and scanner have now been demonstrated on a variety of different bodies and joint designs.

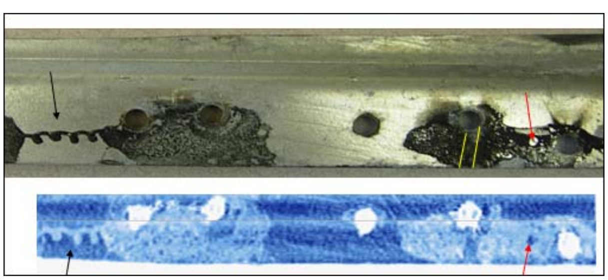

Figure 7. Section from a vehicle (30 mm x 100 mm) with embedded skips. Top image is after peeling; lower PA image is before. The spot welds are readily identifiable.

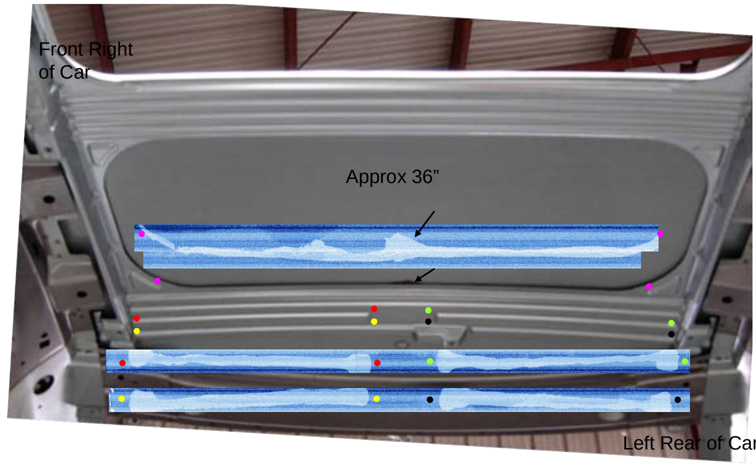

Figure 8. Maps of the adhesive area on a roof bow using the PA probe holder. The colored PA images were obtained on the roof and are superimposed on a picture of the roof bow taken from the vehicle interior.

While already of engineering usefulness, the amplitude C-scans are incomplete. They only register the location of adhesive on the outer adherent. Only with signal analysis can the other interfaces and the thickness be imaged.

The C-scan images are easily interpreted and oriented relative to features on the surface. Furthermore, they can be obtained with simple controllers without signal processing similar images on coupons have been obtained with laser ultrasonics (LU). The primary advantage of using LU is not requiring a water delivery system. However, the production scan rates are currently much lower.

Preliminary Pulse/Echo Signal Analysis

The short burst of high-frequency sound waves travel through the material with some loss of energy and is reflected at any interface. The reflected signal is captured and then analyzed to define the presence and location of reflected surfaces. Variations in reflectivity or scattering can be used as the basis of flaw detection. Transit times of the echoes can be used to assess bond-line thickness. SNL contracted with the Lawrence Livermore National Laboratory (LLNL) to determine if there was any unique signal processing and analysis that could determine adhesive thickness. The LLNL algorithm processes an ultrasonic echo that has many cycles and yields an output that is narrower with respect to time. The ideal output is to reduce multiple complex echoes to a series of delta functions. This would allow small echoes from secondary adhesive interfaces to be resolved. This LLNL algorithm has been used successfully on single interfaces, but not on layered structures with multiple echoes. Figure 9 displays the "golden standard" data to the LLNL algorithm and shows that adhesive thickness is not resolved. There is no uniformity in the data.

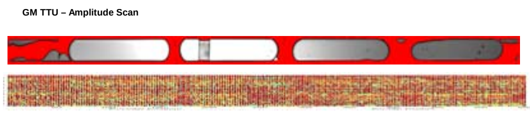

Figure 9. Comparison of through-transmission ultrasonics (TTU) data to the LLNL algorithm.

PA Signal-Analysis and Data Processing

A second, more successful, algorithm repeatedly subtracts a model waveform from a data waveform in a least-square fashion to remove the primary echoes from the first interface. The subtraction attempts to extract the relatively weak echoes associated with the secondary interfaces. Particular care was given to develop an algorithm that uses as few computations as possible and being applied thousands of times in only a few seconds.

The algorithm assumes the primary echoes have a single reflectivity, a fixed round-trip delay time, and minimal frequency dispersion. With these assumptions made, two signals are considered. The first is called the "model" signal, which is the waveform acquired when it is known that no adhesive is present (Figure 10). The second is called the "data" signal, which is associated with adhesive present (Figure 11).

These example signals are from the PA system. The overlapping signals represent the peak values of multiple echoes from model and data waveforms. When adhesive is present, peak values are reduced due to the lower reflectivity. Secondary echoes are typically 10-25% of the peak echoes depending on the adherent.

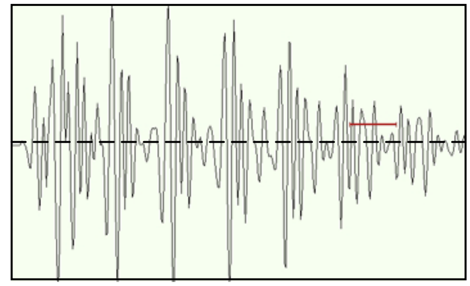

Figure 10. Representative pulse/echo signals on a test specimen – no adhesive present.

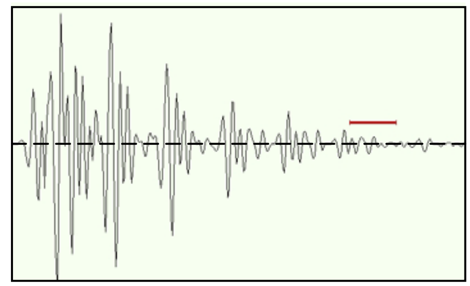

Figure 11. Representative pulse/echo signals on a test specimen – adhesive present.

Finally, the third year of the project will analyze all the inspection data to determine if any data fusion (combining inspection data from two types of inspections) will be achievable.

Completed Assessment of Pulsed Thermography

This technology uses thermal gradients to analyze the physical characteristics of a structure for internal non-uniformity. Flash lamps heat the surface of the structure and the heat diffusion is measured by imaging the surface temperature with a fast-cycle-time infrared camera. Areas that appear hotter or cooler may indicate the presence of a flaw beneath the surface (heat diffusion into deeper layers). By analyzing the time-history of the infrared signal, subtle variations can be enhanced in the image. By plotting the log of temperature versus log of time, quantitative adhesive bond-line thickness measurements were obtained (Figure 12). Additional information about this inspection technique and sample preparation can be found in the first year reports [2, 3].

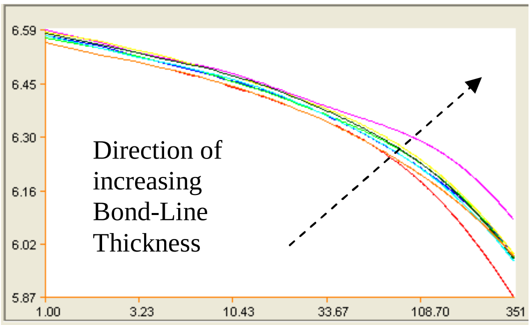

Figure 12. Log of temperature vs. log of time depicts thickness variations on an uncured steel stackup.

While SNL was conducting pulsed-thermography inspections on BIW vehicles, similar inspections on the flat, adhesively-bonded specimens were being conducted concurrently at Thermal Wave Imaging Incorporated. Unfortunately, the high optical reflectivity and low infrared emissivity of Al and steel typically prohibit a successful pulsed-thermography inspection without adding a black paint to the inspection surface.

New Mexico State University (NMSU) was sent infrared (IR) data files to analyze. C-scans optimized for adhesive/no adhesive contrast were processed to extract relative intensity of the pixels along a data line as seen in Figure 13. The spot welds, adhesive and skips can be distinguished in the data. Unfortunately, adhesive thickness could not be easily extracted without reanalyzing the entire time-history datasets.

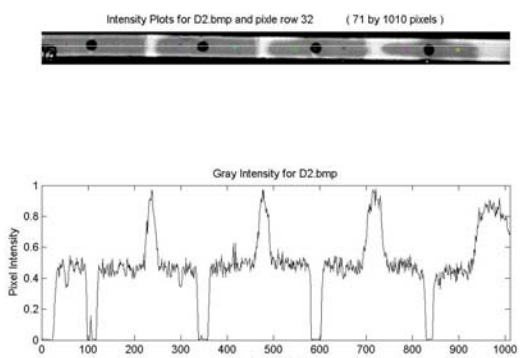

Figure 13. Pixel intensity versus pixel number along the mid-line of an uncured steel stackup.

Inspection of Uncured Adhesives

To date, there has been no difficulty imaging uncured coupons. While the uncured adhesives have a significantly lower speed of sound and are more attenuative, this has not presented a problem so far. In Figure 14, results from the reference UT-TT measurements are shown in comparison with the pulsed-thermography and phased-array pulse/echo measurements. While the thermography results have poorer contrast, the skips, welds, and bead-spread are discernable.

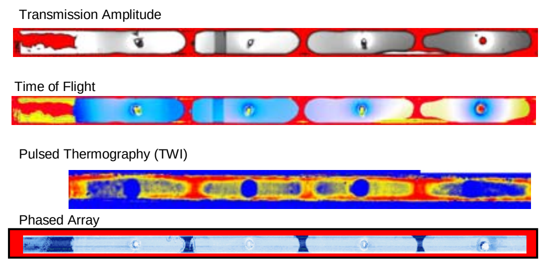

Figure 14. Comparisons of three inspection methods on an uncured-adhesive coupon.

Weak (Kissing) Bond Samples

A procedure to make weak bond samples reproducibly was developed. These used a bearing grease as a model surface contaminate. Figure 15 shows the range of lap-shear strengths obtainable for different thicknesses of grease. These adhesives are designed to work on greasy surfaces and major contamination is needed to affect the strength. These samples were also ultrasonically imaged. The ultrasonic data could be processed to predict the strength with good confidence.

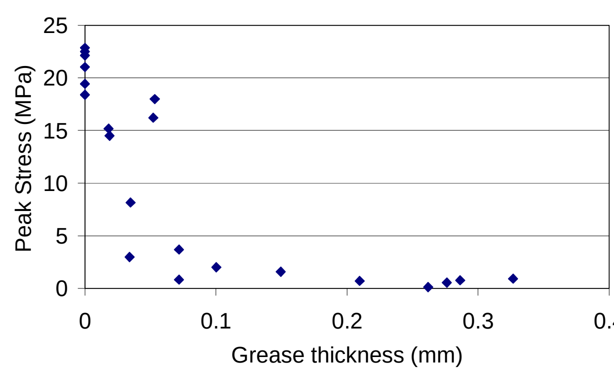

Figure 15. Weak bond shear-strength as a function of grease-contaminate thickness.

Conclusions

Good progress was made on the project objectives during this first full year. An effective inspection tool for off-line inspections was designed, verified, and tested on production vehicles. While this ultrasonic array system is currently only able to inspect the wet-out on the outer skin, the system performance appears to be adequate to allow the adhesive thickness and second interface inspection of 2-layer stickups as signal processing improves. A second-generation version of this ultrasonic array scanner is under development to improve the performance on curved surfaces. A new, high-resolution, wedge-peel test was developed and used to obtain strength scaling laws. Finally, promising results were obtained on the weak-bond samples in the presence of a grease-contaminate.

Acknowledgements

This project team consisted of members from the automobile industries, federal research laboratories and universities. The team members were: Ciji Nelson, Kirk Rackow, Steve Younghouse, Kim Lazarz, Dan Ondrus, Dave Biernet, Jessica Schroeder, John Fickes, Ray Bis, Mike Golden, Dave White, Rajat Agarwal, Bill Brown, Kent Wen and Marvin Klein. We also would like to thank IOS and Olympus NDT for their input and Metal Steel and Novellis for supplying metal blanks.

References

1. Disclosure of Technical Advance Dated February 20, 2007, "*Probe Deployment Device for Optimal Ultrasonic Wave Transmission and Area Scan Inspections*", Joseph DiMambro, Dennis Roach, Kirk Rackow, Ciji Nelson, Sandia National Laboratories and Cameron Dasch General Motor Corporation.
2. NDE601-FY2006 Annual Progress Report for DOE ALM, Joseph DiMambro and Dennis P. Roach Sandia National Laboratories, Cameron J. Dasch General Motors Research & Development, December 15, 2006.
3. "Preliminary Report of Sample Preparation and Ultrasonic Through-Transmission Images of Flat, Mild Steel Coupons for USCAR /USAMP Project NDE 601 – NDI of Adhesive Metal Bonds", *C. J. Dasch, A. Terry, W. Brown, R. Bis, D. White, and D. Sigler*, January 31, 2007.

Presentation/Publications/Patents

1. "Preliminary Report of Sample Preparation and Ultrasonic Through-Transmission Images of Flat, Aluminum Coupons for USCAR /USAMP Project NDE 601 – NDI of Adhesive Metal Bonds", *C. J. Dasch, A. Terry, W. Brown, R. Bis, D. White, and D. Sigler*, February 14, 2007.
2. "Automotive Lightweight Materials: the Roles for NDE in Bringing New Materials into Production", *C. J. Dasch*, Plenary Lecture, Conference on Quantitative Nondestructive Evaluations, Golden, CO, July 2007.
3. "Nondestructive Inspection of Adhesive Bonds in Automotive Metal/Metal Joints (NDE 601)", C. J. Dasch, USAMP Off-site Review, Oct. 25, 2007.
4. "Correlating Adhesive Bond Strength with Non-Destructive Test Methods", K. Lazarz, C. Dasch, R. Agarwal, to be presented at the Annual Meeting of the Adhesion Society, Austin TX, Feb. 2008.

[i] Denotes project 601 of the Nondestructive Evaluation Working group of the United States Automotive Materials Partnership (USAMP), one of the formal consortia of the United States Council for Automotive Research (USCAR, www.uscar.org) set up by Chrysler, Ford and General Motors to conduct joint, pre-competitive research and development.

C. Laser-Ultrasonic Inspection of Adhesive Bonds Used in Automotive Body Assembly

Principal Investigator: Marvin Klein
Intelligent Optical Systems
2520 West 237th Street
Torrance, CA 90505
(424) 263-6361, fax: (310) 530-7417; e-mail: mklein@intopsys.com

Technology Area Development Manager: Joseph A. Carpenter
(202) 586-1022; fax: (202) 586-1600; e-mail: joseph.carpenter@ee.doe.gov

Contractor: Intelligent Optical Systems
Contract No.: DE-FG02-06ER84545 Small Business Innovative Research (SBIR) and Small Business Technology Transfer (STTR) Program

Objective

- Adhesive bonding is widely used in automotive production, especially for body assembly. It is critical to be able to measure the strength of adhesive bonds during manufacture in a nondestructive, effective and rapid manner. There is no current means for inspecting these bonds in real time. The specific inspection requirement is to (1) map the adhesive spread, (2) measure the thickness over the full area, and (3) measure the bond strength. All inspections must be performed from one side and must be able to function on contoured surfaces with ~1 mm resolution. The ideal tool must be able to perform the above measurements simultaneously (i.e., in one pass across the bond). In this project we have applied the technique of laser ultrasonics to the adhesive-inspection requirements described above. The specific goals of this project are to determine the best inspection configuration and signal-processing approach, followed by the development and demonstration of a prototype inspection system.

Approach

- The technology which we will apply to this inspection requirement is laser ultrasonics, in which a pulsed laser beam is directed to the surface to generate ultrasonic waves in the sample, and a continuous-wave laser receiver is used to detect the waves after they interrogate the required sub-surface feature and return to the surface. Laser-based ultrasonic inspection has a number of benefits over transducer-based ultrasonic inspection, including 1) lack of physical contact with the workpiece; 2) high spatial resolution obtained using focused laser beams; 3) high scan rate associated with rapid beam scanning, and (4) high bandwidth, thereby improving the measurement accuracy.

- This project is closely coordinated Sandia National Laboratories' phased-array project, "Nondestructive Inspection of Adhesive Metal/Metal Bonds," funded by DOE and managed by the USCAR Nondestructive Evaluation (NDE) Working Group. (See 10.B) That USCAR-managed project has produced a large number of adhesive-bonded specimens. The flat specimens vary in adhesive, adherent type and thickness, stackup (2-3 layers), cure state, and surface contaminants. These conditions bound the processing parameters for the adhesive assembly process. These specimens have been used to optimize the beam configuration and signal-processing techniques. The remaining portion of our project is devoted to the development and demonstration of a prototype scanning inspection system that can be scaled to a measurement speed of 1 meter/minute.

Accomplishments

- In 2007, we completed a 6-month SBIR Phase I project, as well as three months of a 24-month SBIR Phase II project that started during the year. During the course of this effort, we tested six of the USCAR specimens, thereby enabling us to determine the configuration of both laser beams (separation, size, shape, energy) that provides the best signal-to-noise. We also investigated several algorithms for processing the raw signals to provide mapping and thickness, and selected one of these for further development. We developed a specification for a scanning prototype system and began the associated hardware development.

Future Direction

- In 2008 we will complete the signal processing algorithm development and continue to develop prototype system hardware. The major elements of the hardware development will include implementation of robot scanning, along with associated control software. A measurement head that provides the required beam configuration at the workpiece surface will also be designed and tested.

Introduction

Adhesive bonding is widely used in automotive production, especially for body assembly. The most common use is the lap joining of two or three sheet-metal panels. Adhesive bonding adds strength, and thus allows the use of lighter components at equal performance. Adhesive bonding allows the joining of dissimilar materials such as aluminum (Al) and steel. Modern adhesives (especially epoxy resins) have excellent fatigue and thermal shock resistance and less critical design tolerances because of their gap-filling capabilities. Their service range extends from space environments to high temperatures. It is critical to be able to measure the strength of these bonds during manufacture in a nondestructive, effective, and rapid manner.

The most important manufacturing issues that can influence the strength of an adhesive bond are the maintenance of the proper fit-up and proper surface preparation. While adhesive bonds are tolerant of some range of gap between the panels, if the gap is too large, the adhesive will not cover the required area, and the intrinsic strength of the adhesive itself is reduced. If surface contamination (e.g., oil, grease, surface oxides, corrosion, water infiltration) is present, the bond adhesion will be reduced. In the limit of very low adhesion, weak bonds may have intimate contact, but little or no bond strength ("kissing").

The corresponding requirements for nondestructive evaluation of adhesive bonds fall into three areas: (1) mapping of the adhesive coverage, (2) measurement of adhesive thickness, and (3) measurement of the adhesion of each metal/adhesive bond.

All inspections must be performed from one side and must be able to function on contoured surfaces. The ideal tool must be able to perform the above measurements simultaneously (i.e., in one pass across the bond).

At the current time, nondestructive inspection is not performed during the bonding process. The only quality control techniques now implemented are careful process control, machine-vision inspection of the adhesive bead before joining, and selective destructive evaluation. A nondestructive technique for in-line measurement of adhesive integrity would reduce scrap and warranty costs, and thus allow wider use of adhesive joining.

Laser ultrasonics offer an attractive approach for nondestructive evaluation over a broad range of applications. The full complement of ultrasonic waves (longitudinal, shear, Lamb and Rayleigh) can be produced with known directionality. The pulses are high in bandwidth, thereby providing the high depth resolution required for thin sheets and bonds. The spot sizes on the part can be much less than 1 mm in diameter, thereby providing high spatial resolution.

The objective of this project is to develop a real-time system for inspection of adhesive panels during auto body assembly (see Figure 1). This system will incorporate a fiber-delivered robotic measurement head containing a scanning mirror that will be able to scan narrow sections of adhesive very rapidly.

Samples Provided

General Motors and the USCAR project were kind enough to provide a number of samples for testing. As shown in Figure 2, Samples A1 (uncured) and A3 (cured) consist of a two-sheet stackup with three adhesive joints distributed along the length of the samples, each joint having a spot weld near the center. The middle adhesive joint also contained a section of Teflon tape to simulate a kissing bond. The adhesive is Dow Betamate

1480, a crash-stable epoxy with a longitudinal wave velocity of 2.2 mm/µs in the cured state.

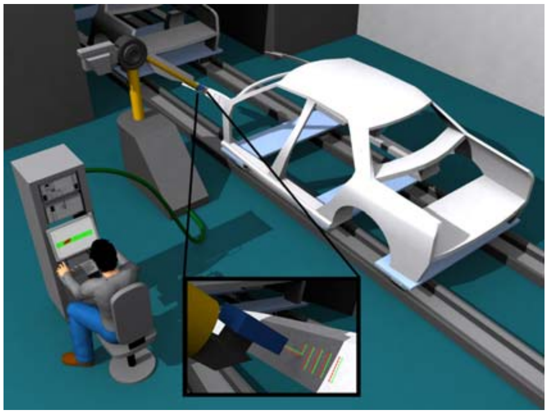

Figure 1. Depiction of robot-driven inspection system performing a two-dimensional scan of an adhesive-bonded auto body panel.

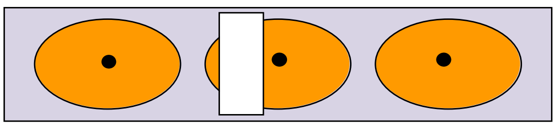

Figure 2. Schematic layout of Samples A1 and A3, showing the thickness for each sheet.

Sample Scans

Typical maps or C-scans of the center portion of Sample A3 are shown in Figure 3. The amplitude map captures the adhesive spatial coverage and detects the presence of the (unbonded) section of Teflon tape. The time-of-flight map contains grey-scale variation that is indicative of the varying thickness of the adhesive. In this latter map, the areas with no ultrasonic arrivals (no adhesive or Teflon tape) appear with random amplitude, as the software is processing only noise.

The maps in Figure 3 were taken with 3-mm steps to speed the data acquisition. An amplitude zoom scan of the left portion of Figure 3 with 1-mm step size is shown in Figure 4. The edges of the adhesive are now resolved to a level required for factory implementation.

All subsequent measurements were performed with both beams on the same side (pitch-catch configuration) and spaced 1-2 mm apart. In this configuration, multiple echoes are expected from both the A and B interfaces (with A the adhesive

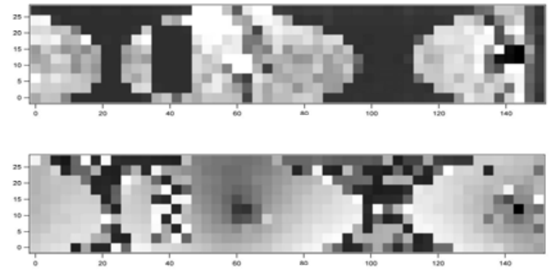

Figure 3. Through-transmission C-scans of Sample A3 based on amplitude (top) and time-of-flight (bottom). Step size=3 mm.

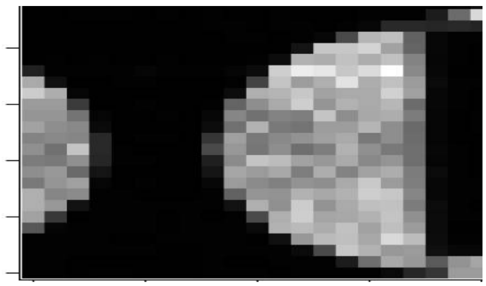

Figure 4. Zoom image of left portion of Figure 3 (top). Step size=1 mm.

interface closest to the measurement head and B the adhesive interface furthest away from the measurement head). The value of the reflectivity at these interfaces is dependent on the impedance values of each material. Specifically, the reflectivity of a steel/adhesive interface (~0.9 in amplitude) is smaller than that of a steel/air interface (very close to 1.0). This difference is not large, but it is sufficient to yield a measurable difference in the amplitude of the interface echoes. We also expect that phase changes could alter the shape of the arrivals. We wish to use these characteristic changes as a means of mapping the adhesive.

In Figure 5, we show a B-scan on sample F14 in which the beams pass over a gap in the adhesive between position x=-9 mm and x=+9 mm. A B-scan is a grey-scale plot of the detected signal at a series of one-dimensional (1D) positions along the sample. Our beam configuration produces very strong multiple reflections in the front sheet. As indicated above, the reflection coefficient from the back surface of the front sheet is slightly larger when adhesive is absent than it is when adhesive is present. Thus, the reflected wave amplitude is larger over the gap, and the difference from the adhesive areas increases with each reflection. This effect is clearly visible in Figure 5. The clarity of this difference is directly associated with the optimized beam configuration that we have determined. In spite of the clear amplitude difference in Figure 5, it is risky to rely on amplitude as an indicator of the spread of adhesive, as many other experimental factors can change the amplitude and possibly give a false positive indication. The next section discusses an alternative and preferred approach to mapping the adhesive.

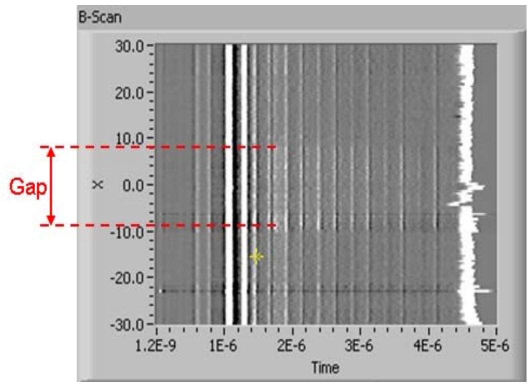

Figure 5. B-scan across 60 mm on Sample F14.

Signal-Processing Development

The objective of our signal-processing development is to amplify the features in the signals which allow direct measurement of the adhesive spread with requiring a direct measurement of signal amplitude. Specifically, we wish to identify the transition regions at the edges of the adhesive. We have applied a number of digital signal-processing techniques to enhance the edge signals in our scans. In Figure 6, we show an example of a processed B-scan using the data plotted in Figure 5. Now the transition regions are identified as changes in sign of the backwall echoes are small shifts in the arrival times. These features are not dependent on variations in the amplitude of the echoes and are thus much more robust for automated processing.

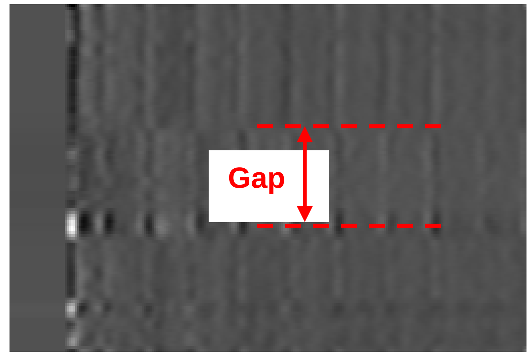

Figure 6. Processed and expanded B-scan using the data shown in Figure 5. Based on the time scale in Figure 5, the time span in Figure 6 extends from 1.5 to 4 microseconds.

Scanning-Head Development

The scanning head has two main components: the measurement head, and the generation laser-coupling module. The measurement head is diagrammed in Figure 7. The generation beam is delivered through a fiber bundle, while the probe beam is delivered through a conventional fiber. The beams are combined at a dichroic beam combiner and then focused onto the adhesive panel surface. The beams are separated on the surface by a few millimeters. The return probe light from the surface is collected and delivered to the signal fiber for later processing. The measurement head has been designed for ease in assembly and alignment.

In Figure 8 we show a top view photo of the assembled head.

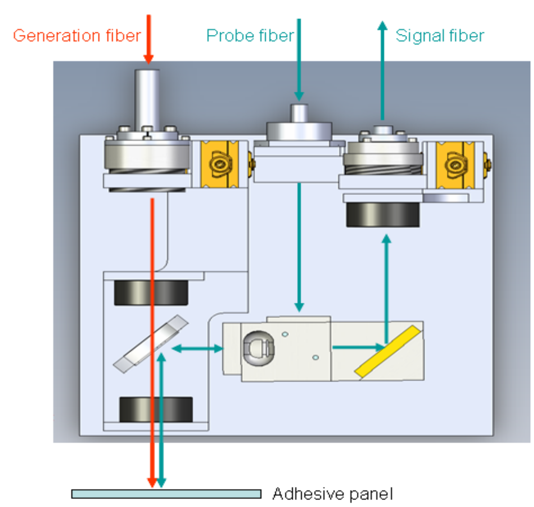

Figure 7. Schematic drawing of measurement head.

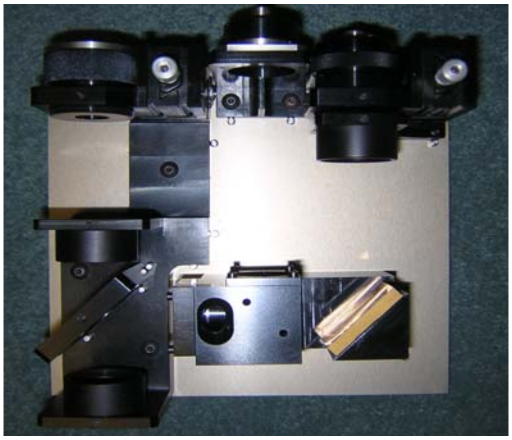

Figure 8. Top view photo of assembled head with cover removed.

The generation laser pulses can easily damage a fiber if not controlled carefully. In order to eliminate the risk of damage, we use a fiber bundle to deliver this beam to the measurement head. A proprietary optical module is used to couple the generation laser beam into the fiber bundle.

Conclusions

In 2007, we completed an SBIR Phase I project and started a Phase II project. Good progress was made on the overall project objectives.

We have successfully applied laser ultrasonics to the requirement for evaluating adhesive bonds used in auto body assembly. Techniques have been developed to map the adhesive spread and measure the thickness. The signal processing efforts have indicated a pathway for processing the raw data in real time. We have designed prototype scanning hardware that will be robot-mounted for automated measurements. Continued work in 2008 will be required to refine the signal processing and test/improve the measurement hardware.

Presentations/Publications/Patents

None.

D. In-Line Resistance Spot Welding (RSW) Evaluation System for Lightweight Materials

Project Leader: William Charron
Ford Motor Company
6100 Mercury Drive, Dearborn, MI. 48126
(313) 805-6628; e-mail: wcharron@ford.com

Principal Investigator: Xin Sun
Pacific Northwest National Laboratory (PNNL)
P.O. Box 999/K2-03, Richland, WA 99352
(509)375-6489; fax: (509) 375-2604; e-mail: xin.sun@pnl.gov

Project Technical Administrator: Todd Cleaver
Tech Knowledge
(734) 675-5562; fax: (734) 675-5562; email:toddcleaver@wowway.com

Technology Area Development Manager: Joseph A. Carpenter
(202) 586-1022; fax: (202) 587-1600; e-mail: joseph.carpenter@ee.doe.gov

Expert Technical Monitor: Philip S. Sklad
(865) 574-5069; fax: (865) 576-4963; e-mail: skladps@ornl.gov

Participants:
This project is being conducted as a partnership with the Automotive Metals Division (AMD) of the U.S. Automotive Materials Partnership (USAMP) with participation that includes (but is not limited to) the following automotive company representatives:
Bill Charron, Ford Motor Company
Dan Cerjanec, Chrysler Corporation
John Bohr, General Motors Corporation

Contractor: PNNL
Contract No.: DE-AC06-76RL01830

Objectives

- Assess the current state-of-the-art for in-line resistance spot welding (RSW) control and evaluation systems and determine their potential for application to direct weld control for lightweight sheet materials.
- Determine feasibility of the most promising control technologies to overcome the primary technical hurdle, accurate identification of key weld characteristics and all weld defects that occur in the production process (during nugget formation or immediately thereafter).
- Assess the control technologies for probability to meet performance, business, and retrofit/integration targets.

Approach

- Develop assessment criteria and performance targets for weld quality, cost, and retrofit/integration potential. A team of original equipment manufacturer (OEM) welding experts will participate in this task and establish a test protocol for an “apples-to-apples” comparison of systems which will be used to assess evaluation systems currently available for testing.

- Suppliers/developers of in-line RSW control and evaluation systems will be invited to participate and subject their systems to the proposed assessment.
- Samples of the full range of potential defects will be made for control systems that require them. Each system will process selected lightweight sheet materials and thickness combinations.
- Data and system outputs will be captured, evaluated, measured, and assessed against the criteria/targets established by the team and identification and recommended next development steps (if any) will be reported.

Recent Accomplishments

- Developed business-issues questionnaire for in-line adaptive and post-weld audit systems.
- Developed test protocol for in-line adaptive and post-weld audit systems.
- Identified the materials needs and material availability.
- Identified the full list of potential system suppliers.
- Invited potential system suppliers to participate in testing and complete the business-issues questionnaire.

Future Direction

- Project terminated.

Introduction

Aluminum (Al) and advanced high strength steel (AHSS) sheet materials represent substantial opportunities to save weight and improve fuel efficiency. Robust spot-weld control and quality assessments are significant hurdles in the accomplishment of widespread implementation of these materials. This project assesses the current state-of-the-art for in-line RSW control and evaluation systems and determines their potential for application to direct weld control for lightweight sheet materials.

No economically-reliable method exists today to inspect RSWs at production rates. The currently accepted practices make use of labor-intensive, manual teardown inspection processes, performed every shift to determine weld quality off-line. In addition, in-line manual pry checking is performed on selected joints. Pry-testing and teardowns do not allow plant management and engineers to collect inspection data that allow them to identify trends and potential problems or make pre-emptive adjustments to the weld systems prior to defect identification. And, these practices result in significant cost, quality, productivity, and safety/health issues and always occur many cycles after the welds have taken place.

Furthermore, these inspection techniques are not viable options for advanced, lightweight, thinner-gage AHSS and Al materials. As the industry moves toward body structures with more AHSS and Al, the post-mortem teardown inspection processes for weld integrity will be less reliable and more difficult and costly, potentially discouraging the implementation of these materials. The pry-test procedure may not work at all with AHSS materials or damage the material as is the case with Al sheet. Clearly, a new method is required to assure that high-quality welds have occurred.

Several OEMs and suppliers have attempted to develop technologies (ultrasonics, infrared [IR] thermography, artificial intelligence, etc.) to resolve these problems. However, concept feasibility has not been demonstrated for many of these developments and even fewer have been evaluated in OEM test facilities or on production lines. The lack of comparable measurables for these systems hampers a clear understanding of the technical hurdles to be overcome (if any) before any systems can be deployed with any confidence. In the final analysis, widespread usage of this technology in the domestic automobile industry will depend on the ability to 1) identify all weld defects (during nugget formation or immediately thereafter); 2) develop robust control algorithms; 3) retrofit/integrate into existing weld controllers; and 4) provide affordable technology. The objectives of the current concept-feasibility study are: 1) determine feasibility of the most promising control technologies to overcome the primary technical hurdle, i.e., *accurate identification of key weld characteristics and all weld defects that occur in the production process* (during nugget formation or immediately thereafter) and 2) assess the control technologies for probability of meeting performance, business, and retrofit/integration targets. Upon successful completion of this project, a follow-on effort may be proposed to resolve identified technical hurdles of the most promising control systems.

This effort is an essential first step in understanding what control and assessment technologies/ approaches are appropriate for maturation and application in spot-welding lightweight materials. This work will lead to better understanding of the welding process resulting in improved consistency, optimization and control. And, it may offer the potential to reduce the number of welds and associated manufacturing costs and facilities. In summary, development of in-line evaluation and control techniques is an enabling technology for greater use of lightweight materials such as AHSSs and Al, in the automotive industry where systems to assure product quality are essential for industry and consumer acceptance of new materials and manufacturing methods. This project, a collaboration between USAMP AMD and PNNL, started in December of 2006.

Development of Business-Issues Matrices for In-line Adaptive and Post-Weld Audit Systems

During the first quarter of the project, the project team met regularly and developed the business-issues matrices and technology-issues matrices for both the in-line adaptive and post-weld audit systems (Refs 1-2).

For example, the business issues matrix for the in-line adaptive systems include scores for 19 (nineteen) categories including the individual system's stage of technology, product capital cost, process time per weld, etc. See Table 1. These scores will help OEMs in understanding and building a case for business-related concerns to measure/evaluate impact to incumbent operations that may affect implementation and adoption of the technologies.

Supplier/system name	Input			Comments
Stage of technology		1-5	1 being at research level	5 being commercial ly available
Product capital cost ($)/system			From supplier	Best-faith-estimate based on purchase of 20 units
Process time/weld			Measured	
Product life cycle (years)			From supplier	
Warrantee coverage (years)			From supplier	
Maintenance frequency (#/shift)			From supplier	What & how often
Calibration frequency (days)			From supplier	
Cost and time to calibrate			From supplier	
Non-contact or contact		1 or 0	1 for non-contact	0 for contact
Portability (weight in lb.)		1 or 0	1 portable	0 non - portable
Personnel training cost				
Operator skill level		3 = non-skille d	2 = skilled	1 = technician 0 = engineer
Programming cost and set up time to launch			From supplier	
Safety and ergonomics		1-5		
Roster of current applications				
References for each application locations				
List robot your system HAS interfaced with				
List robot your system CAN interface with				
Adaptive to servo guns?				

Table 1. Business-isues matrix for in-line adaptive systems

The potential supplier list for the in-line adaptive system included nine commercial suppliers, the three OEMs and DOE's Oak Ridge National Laboratory [ORNL] and Lawrence Berkley National Laboratory [LBNL].

The materials considered include:

a. Bare mild steel
b. Hot-dip (HD) galvanized mild steel
c. Galvanneal mild steel
d. Coated high-strength low-alloy (HSLA)
e. Bare transformation-induced plasticity (TRIP)
f. HD galvanized TRIP
g. Galvanneal TRIP 800 or coated dual phase (DP) 800
h. Boron steel
i. Al alloy xxxx (TBD)

Development of Test Protocol for In-line Adaptive and Post Weld Audit Systems

Weld sample fabrication protocols have been established for the two different types of systems due to the intrinsic difference in inspection and control philosophy.

Audit Systems

For the audit systems, a two-step procedure is used in which the first step involves sample fabrication and the second step is actual inspection. Sample-fabrication process will generate the desired fusion-zone size distribution as well as the desired types of weld defects in order to test the capabilities of the inspection systems.

The ground rules for the inspection procedure are then developed for all the participating systems:

- All participants/system suppliers will be provided representative training sets for machine set up.
- All participants/system suppliers will be evaluating the same welds, both on the coupon level and on the component level, i.e., a production door or other selected production part.
- After all the samples are evaluated by all the system suppliers, X-ray, peel tests and metallographic cross sectioning will be performed to quantify various weld attributes.
- For each supplier system, the following measurements will be recorded and compared with actual destructive measurements:
  - Maximum fusion-zone diameter
  - Minimum fusion-zone diameter
  - Fusion zone penetration
  - Weld indentation
  - Amount of weld porosity
  - Amount of weld cracks

Table 2 shows the weld-quality quantification Table A for each weld population and system supplier. Consolidated data for each supplier for all the weld populations will then be captured in Table 3 for overall system evaluations.

In-Line Adaptive Systems

The control capability of in-line adaptive systems will be examined under both perfect and imperfect welding conditions. The imperfect welding conditions include:

a. Electrode wear/mushrooming
b. Gap
c. Edge weld
d. Shunting
e. Sealant

In order to efficiently examine the capability of weld-quality control systems under these different welding conditions, a coupled welding procedure is developed in which 554 welds are made for each weld population. Out of the 554 welds, 72 will be cross sectioned, 72 will be peeled. All the rest of the welds are performed to simulate electrode wear conditions. For details, please refer to the testing procedures listed in Ref. 2.

Ground rules for sample fabrication procedures for the in-line adaptive systems are determined; once the system is set-up for one population, no adjustments are allowed while making all the 554 welds for that population. Details follow the document from AMD 303.

All the system measurements will be compared with destructive weld attributes measurements such as metallographic cross-sectioning and peel tests. For each supplier, the following parameters will be compared for each weld between the specified value and the actual destructively tested value:

- Maximum fusion-zone diameter – target values per American Welding Society (AWS) D8.1M or AWS D8.2M (Refs. 3-4)
- Minimum fusion-zone diameter -- target values per American Welding Society (AWS) D8.1M or AWS D8.2 (Refs. 3-4)
- Fusion-zone penetration – Target minimum values to be determined

- Weld indentation – Target allowable values to be determined
- Expulsion
- Weld porosity
- Weld cracking

Supplier/System Name:																		
Weld population ID:																		
Weld No.	Max fusion-zone diameter (mm)			Min fusion-zone diameter (mm)			Weld indentation (mm)			Weld penetration (mm)			Weld porosity definition (%)			Weld cracking definition (%)		
	System measured	Destructive test	Deviation from NDE to actual destructive measurement α (mm)	System measured	Destructive test	Deviation from NDE to actual destructive measurement β (mm)	System measured	Destructive test	Deviation from NDE to actual destructive measurement γ (mm)	System measured	Destructive test	Deviation from NDE to actual destructive measurement ζ (mm)	System measured	Destructive test	Deviation from NDE to actual destructive measurement ψ (%)	System measured	Destructive test	Deviation from NDE to actual destructive measurement η (%)
1																		
2																		
…																		
20																		
Average deviation																		

Table 2. Weld-quality quantification Table A for audit system.

Supplier/System name:									
Can max and min fusion zone diameters be measured?	1 or 0: Yes- 1, No- 0								
Can weld penetration be measured?	1 or 0: Yes- 1, No- 0								
Can weld indentation be measured?	1 or 0: Yes- 1, No- 0								
Can weld porosity be measured?	1 or 0: Yes- 1, No- 0								
Can weld cracking be measured?	1 or 0: Yes- 1, No- 0								
Deviations (α-η) from Table A or correlations (χ) from Table B			α	β	γ	ζ	ψ	η	χ
System measurement accuracy	TRIP or DP	2-t stack							
	Boron steel	2-t stack							
	aluminum alloy	2-t stack							

Table 3. Weld-quality quantification Table B for audit system.

For each weld population, Table 4 will be filled out for systems that are able to control the above seven parameters. For systems that do not control certain attributes, that column will be keyed in as 'NA'. The numerical results from Table 4 will then be used as inputs for each row in Table 5 to consolidate the results for each supplier.

The weld acceptance criteria documented in the new AWS standards (Refs. 3-4) are used to define the attributes for acceptable welds. All the suppliers in the adaptive-controls category are subjected to the same testing and evaluation conditions.

Identification of Materials Availability

Initial material-availability search has been conducted inside other project teams within USCAR, Auto Steel Partnership (A/SP) and among OEM and suppliers. Corresponding material needs have been calculated and the weld population definitions have also been drafted.

Sources for all the materials needed for the project have been identified. These sources include: Chrysler, General Motors, A/SP Inventory, and steel suppliers.

Project Execution

After the business-issues questionnaires and test protocols for both the in-line adaptive and post-weld audit systems were developed, they were sent to 15 system suppliers with an invitation to participate. The survey used the commercial website called 'Survey Monkey.' Because of sensitivity of data requested, individual questionnaires were held in confidence and not shared with competitors. The questionnaires surveyed the following topics on individual systems:

- Calibration
- Maintenance
- Training
- Launch
- Cost
- Development Needs
- Cycle Time
- Commercial Availability
- Portability
- Robot Interface

Supplier/System Name:															
Weld population ID:															
Weld measurements	Max fusion-zone diameter (mm)			Min fusion-zone diameter (mm)			Weld indentation (mm)			Weld penetration (mm)			Porosity	Expulsion	Cracking
	Specified/ requirement	Destructive test	Deviation from actual measurement to requirement α *(mm)	Specified/ requirement	Destructive test	Deviation from actual measurement to requirement β *(mm)	Specified/ requirement	Destructive test	Deviation from actual measurement to requirement γ (mm)	Specified/ requirement	Destructive test	Deviation from actual measurement to requirement ζ *(mm)	No- 0 Yes- 1	No- 0 Yes- 1	No- 0 Yes- 1
1															
2															
3															
…															
9															
Average deviation															

Table 4. Weld-quality quantification Table A for RSW adaptive systems.

Supplier/System name:							
Control accuracy (α-ψ) from Table A	α	β	γ	ζ	χ	η	ψ
Electrode wear							
Gap							
Edge weld							
Shunting							
Sealant							

Table 5. Weld-quality quantification Table B for RSW adaptive systems.

Although the initial responses at the project kick-off meeting were overwhelmingly enthusiastic from many suppliers, the feedback to the business-issues questionnaire and testing was sparse. Only four suppliers submitted the questionnaires. Only two suppliers volunteered to participate in the testing of their systems. The remaining suppliers declined to participate.

Both infrared (IR) thermography technology suppliers submitted questionnaires and identified potential technology needs. These needs were identified as measurement accuracy of cracks, porosity and indentation.

Because of the lack of participation from various system suppliers in this stage of the project, the project team concluded that it was no longer possible to meet the project objectives and timeline for deliverables outlined in the Statement of Work (SOW) and decided to stop all development work.

The team then proceeded with project closure tasks and notified AMD and USAMP of team decision.

Conclusions

Technology questions and concerns still remain regarding the feasibility of control technologies to accurately identify key weld characteristics and defects that occur in the production process during nugget formation or immediately thereafter. Furthermore, no viable technologies exist for the inspection and control of RSW for advanced, lightweight, thinner gage, AHSS and Al materials. As a result, as the industry moves toward body structures with more AHSS and Al, the post-mortem teardown inspection processes for weld integrity will be less reliable and more difficult and costly, potentially discouraging the implementation of these materials.

The only technical needs identified in the project for further development consideration were in IR-thermography technology.

References

1. RSW Audit System Evaluation Matrix and Testing Procedure (DRAFT), AMD 605 document, February 2007.
2. RSW Inline Adaptive System Evaluation Matrix and Testing Procedure (DRAFT), AMD 605 document, April 2007.
3. Specification for Automotive Weld Quality – Resistance Spot Welding of Steel, AWS D8.1M-E1-DS1, An American National Standard, American Welding Society, 2007.
4. Specification for Automotive Weld Quality – Resistance Spot Welding of Aluminum, AWS D8.2M, An American National Standard, American Welding Society, 2006.